Available online at www.sciencedirect.com
ScienceDirect
Journal of Sound and Vibration 308 (2007) 855–866
JOURNAL OF SOUND AND VIBRATION
www.elsevier.com/locate/jsvi

Ultrasonic impact peening for the surface properties' management

Bohdan N. Mordyuk*, Georgiy I. Prokopenko

Department of Acoustics of Solid State, Kurdyumov Institute for Metal Physics, National Academy of Science of Ukraine, 36 Academician Vernadsky blvd., 03142, Kyiv, Ukraine

Accepted 28 March 2007
The peer review of this article was organised by the Guest Editor
Available online 25 May 2007

Abstract

It is demonstrated that the ultrasonic impact peening (UIP) technique is a beneficial method for essential increase in the fatigue durability of metallic materials due to the surface nanocrystallization and hardening process provided for severe plastic deformation of surface via multiple impacts of high velocity impact pins. Nano-scale grain structures were obtained in the surface layers of stainless steel, low carbon steel weld and different titanium alloys using developed equipment for the UIP. Both the surface nanostructure and compressive residual stresses are shown to attribute to the essential hardness increase. It is revealed experimentally using profilometry that new modification of the UIP apparatus providing high velocity "sliding" impacts leads to marked diminution of the surface roughness, which is another important factor affecting to the fatigue cracks initiation process. The two-dimensional finite element model is used to simulate the indent formation process during single impaction. The solid steel pin and the Al alloy plate are modeled as a rigid material and an elasto-plastic material, respectively. It is shown that the surface roughness magnitude depends on the correlation of the vertical and lateral load components.

1. Introduction

The materials failure including wear, corrosion and fatigue is well known to be dependent on the material surface state [1,2]. Therefore, improvement in the surface layers' properties by changing their grain structure, hardness, and residual stresses is very actual.

Recently ultrasonic shot peening [3–6] (other name is surface mechanical attrition treatment) with intermediate shot elements, which leads to the surface nanocrystallization and hardening process [7], has been studied, along with traditional shot peening [8,9]. Ultrasonic impact peening (UIP) utilizes another loading scheme [10] consisting in use of steel pins positioned into impact head installed on the ultrasonic horn tip. Recently, the UIP has been successfully used to improve the fatigue life of welded constructions [10,11]. The UIP leads to the most marked fatigue improvement among the other methods for sever plastic deformation

*Corresponding author. Tel./fax: +38(044) 424 0521.
E-mail address: mordyuk@imp.kiev.ua (B.N. Mordyuk).

0022-460X/$ - see front matter © 2007 Elsevier Ltd. All rights reserved.
doi:10.1016/j.jsv.2007.03.054

(SPD) of materials surfaces [12]. Besides, the UIP processing seems could be more controllable in comparison with those SPD methods consisted in random impacting of metallic components by high-energy balls.

For the first time, scientists from different countries independently considered the UIP as one of SPD methods in 70th of last century, viz., Krylov and Polischuk (1970, Russia) [13], Feng and Graff (1972, USA) [14], Prokopenko et al. (1974, Ukraine) [15], and Statnikov et al. (1977, Russia) [16]. Currently, many modifications of apparatus, which use various loading schemes, have been developed and great practical benefits consisting in the enhancement of the materials functional properties have been demonstrated. However, the physical bases of deformation processes during the UIP processing are still in discussion due to the absence of systematic studies for mechanisms of structural evolution and hardening process.

Recently, a novel scheme and device for the UIP were proposed [17], which permit sufficiently homogeneous processing of large flat surfaces. Evenness of the surface structural state, the surface hardness and roughness can be achieved using repetitive high frequency impacts by the processed surface and simultaneous shifting of pin/sample during single impaction [18]. These features can be produced either by rotation of the impact head or rotation/vibration of sample itself. Both contact-shifting conditions during single indentation and multi-directionality of indentations promote essential refinement of grains/crystallites [3,18,19]. It should be noticed also that the rough surface created by SPD methods might mask the beneficial effect of a surface microstructure even in the nano-scale range. Indeed, roughness may induce stress concentration at specific points, thus facilitating crack initiation under fatigue conditions [2,8,20–22]. Therefore, surface mechanical treatments should be performed in regimes, which would provide the lowest surface roughness characteristics. Shot peening or ultrasonic shot peening can produce the lowest surface roughness only after relatively prolonged treatment. On the contrary, markedly reduced treatment time is shown to need for the UIP processing presented in this paper to meet the lowest surface roughness requirements. The surface roughness was studied experimentally by profilometry. Besides, two-dimensional (2D) finite element (FE) model is developed, which describes the indent contours formed on the surface of the Al alloy sample after impaction by a rigid ball.

2. Experimental details

2.1. UIP processing details

The UIP equipment consists of an ultrasonic generator with a frequency of 21 kHz and a power output of 0.6 kW, a piezo-ceramic transducer, a step-like ultrasonic horn made from durable Ti-alloy and the impact head installed on the horn tip. The impact head (Fig. 1) contains cylindrical pin(s) (diameter of 5 mm, length of 18 mm, and mass of 3 g), which may move easily within a gap between the horn tip and the sample surface treated. The pins acquire their kinetic energy from the vibrating ultrasonic horn tip and produce impacts by

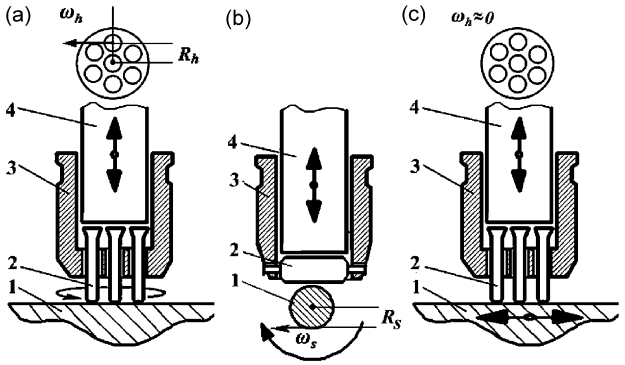

Fig. 1. Impact heads used for the UIP processing of flat (a,c) and round-bar (b) samples: (1) sample, (2) pin(s), (3) head body, (4) ultrasonic horn. ω_h, ω_s are the head/sample linear components of rotation velocities, R_h, R_s are the appropriate radii. Note that in case (c) the lateral load component arises due to low frequency vibrations of the processed sample.

the surface being treated, providing the normal (vertical) component of load. Besides, different processing schemes used in this study (Fig. 1) allow producing the lateral component of load during the pin impaction by the sample surface. Scheme A consists in constrained rotation of the seven-pin head around the horn axis during the UIP processing, while a flat sample is fixed (Fig. 1a) [17,18]. The round bar sample is rotated purposely during the UIP processing with the one-pin head (scheme B—Fig. 1b). Low-frequency generator (50 Hz, the vibration amplitude was of 10 mm) is used additionally in scheme C (Fig. 1c) for constrained vibration of flat samples (including welds) during the UIP processing, while the impact head is fixed.

The basic concept of the UIP of flat surfaces (scheme A) has been described in Ref. [18]. Briefly, in order to treat some area of flat surface in the desirable regime one can choose the following parameters: (i) intensity of ultrasound (the horn tip vibration amplitude), which will actually determine a magnitude of the vertical load component during single impaction; (ii) either the rotation velocity of the impact head (scheme A—Fig. 1a) or amplitude of low-frequency vibration of sample (scheme C—Fig. 1c), which will determine a magnitude of the lateral load component during single impaction; (iii) the shift velocity of the whole acoustic system along the surface (scheme A—Fig. 1a), which will actually determine both the quantity of impacts by the specific surface area and the multidirectionality of impacts during processing.

Processing regimes for the UIP schemes used are listed in Table 1. The mechanical energy P injected per impact [18,23,24] was chosen as a main parameter in order to normalize different UIP schemes. It can be estimated considering the fact that pins acquire their kinetic energy (E_k) from the vibrating ultrasonic horn tip (E_{us}) (vibration frequency f_{us} and amplitude ξ), from the rotary motion of the impact head/sample (E_r), or from low-frequency vibration of sample (E_{lfv}) (vibration frequency f_{lfv} and amplitude A) using the following expression:

$$P(W/g/\text{impact}) = \frac{f_i E_k}{m} = \frac{f_i}{m}(E_{us} + E_a) \approx \frac{f_i}{m}\left[2\pi^2 f_{us}^2 \xi^2 m_p + E_a\right], \tag{1}$$

where $f_i \approx 3 \pm 0.5$ kHz [24] is a frequency of impactions, m is a coefficient with the mass dimension, which takes into account the correlation between the pin mass m_p and the sample mass m_s, E_a is an additional kinetic energy, which can be evaluated for different cases as follows:

$$\text{for rotation of head or sample (schemes A or B)}: \quad E_a = \alpha(n\pi R^*)^2 m^*, \tag{2a}$$

$$\text{for low} - \text{frequency vibration of sample (scheme C)}: \quad E_a = 2\pi^2 f_{lfv}^2 A^2 m_s, \tag{2b}$$

where n is a swiftness of head/sample per second, asterisks at R^* and m^* indicate that R_h or R_s and m_p or m_s should be chosen in appropriate case. Here R_h is the path radius of the pin motion (distance between pin and the head rotation axis (Fig. 1a)) and R_s is the sample radius (Fig. 1b), α is equal to 1 in case of the sample rotation or 2 otherwise.

Since the mechanical energy P injected per impact was purposely sustained equal, it was assumed that processing conditions for samples of all types were similar. Besides, the energy dissipated during impact due to plastic deformation [25] is supposed equal in all considered cases.

Low carbon steel (weld sample), AISI 321 stainless steel and different titanium alloys (VT1-0—close to CP α-titanium Grade 7, VT6 and LCB—$\alpha+\beta$ and β titanium alloys, respectively) were chosen for studies. Flat samples with dimensions $40 \times 20 \times 10$ mm were UIP-processed for further XRD and microhardness

Table 1
Description of the UIP regimes used

UIP Scheme (as in Fig. 1)	Horn vibration frequency, f_{us} (kHz)	Horn vibration amplitude, ξ (μm)	Impact frequency, f_i (kHz)	Sample vibration frequency, f_{lfv} (Hz)	Sample Vibration amplitude, A (mm)	Impact normal (90°) velocity, $\vartheta_\perp$ (m s^{-1})	Impact lateral velocity, $\vartheta_\parallel$ (m s^{-1})
A				—	—		$\vartheta_\parallel = \omega_h = 2\pi n R_h = 5$
B	21	20	3 ± 0.5	—	—	$\vartheta_\perp = \vartheta_{us} = 2\pi f_{us}\xi = 5$	$\vartheta_\parallel = \omega_s = 2\pi n R_s = 5$
C				50	16		$\vartheta_\parallel = \vartheta_{lfv} = 2\pi f_{lfv} A = 4.93$

measurements. Besides, plane-view foils of top surface layers were prepared for transmission electron microscopy (TEM). The standard round-bar hourglass samples were UIP-treated for further evaluations of the fatigue behavior. The UIP processing duration for the schemes used were chosen to provide similar impacts quantity per the sample surface area, that is, $P \approx \text{const}$.

2.2. Structure and fatigue behavior examination techniques

X-ray analysis was carried out using a DRON-4 diffractometer with Co K_α (for Ti alloys) and Fe K_α (for steels) irradiations. Residual stresses $\sigma_1 + \sigma_2$ in surface layer were estimated using the standard routine based on determination of the lattice spacing change (σ_3 was assumed negligible). The micro-hardness was measured using microhardometer PMT-3 at the Vickers' diamond indenter load of 100 g.

TEM observations of structure in the top surface layers were carried out on microscope JEM 100 CX-II. The plane-view TEM foils were obtained first by mechanical polishing on untreated side, it was then one-side electro-polished using a twin-jet technique in a solution of 590 ml CH_3OH, 350 ml $C_6H_{14}O_2$ and 60 ml $HClO_4$ at a voltage of 23–25 V and a temperature of $-40\,^{\circ}C$ (only for Ti-alloys).

High cycle fatigue tests after the UIP were carried out in room-temperature air either using a rotary bending fatigue-testing machine (Model: M1) at a cyclic frequency of 46 Hz for VT1-0 Ti alloy or bending fatigue-testing machine at a cyclic bending of 7 Hz for welded samples of low carbon steel. These tests consist in the fatigue life determination with constant stress amplitude.

2.3. Description of FE model

A 2-D FE model is built to calculate the single indent profile on the sample surface, which is impacted by a rigid pin. The analysis is carried out by commercial FE code MSC.Marc 2005 [26]. The FE model consists of a solid steel ball (ShKh15 steel) impacting the center of the annealed Al alloy plate section (Al-3Mg) with dimensions of $20 \times 5\,\text{mm}^2$ at a velocity in vertical (90°) direction $\vartheta_\perp = 5\,\text{m s}^{-1}$ and a velocity in lateral direction ω ranged within interval $\omega = 0$–$10\,\text{m s}^{-1}$. The Young's modulus, density and Poisson's ratio are 220 GPa, $7.87\,\text{g cm}^{-3}$ and 0.3 for the steel ball, and 70 GPa, $2.7\,\text{g cm}^{-3}$ and 0.3 for the Al alloy plate, respectively [27]. In simulation, the Al alloy plate is modeled as an elasto-plastic material with initial compressive yield strength of 230 MPa [27] and a power-law strain hardening behavior described by the following true stress **S**—true strain **e** relationship:

$$\mathbf{S} = 393\mathbf{e}^{0.12}\text{MPa}. \tag{3}$$

The steel ball is modeled as a rigid material because it is much harder (HB = 6010 MPa) than the annealed Al alloy plate (HB = 750 MPa). All the nodes are free to move in X, Y directions except the nodes at the bottom, which are fixed. The friction between pin and plate is not considered yet. The Al alloy plate is assumed strain-rate insensitive. To ensure the calculation accuracy, the mesh in the region being impacted by the ball is much finer than that in edge regions. The square elements' dimensions in the impacted region are $0.03 \times 0.03\,\text{mm}$.

3. Experimental results and discussions

The XRD analysis of AISI 321 stainless steel and VT1-0 alloy samples after the UIP reveals both displacement and significant broadening of diffraction peaks in comparison with those for untreated samples. The displacement of diffraction lines toward lower diffraction angles revealed is known to be equivalent to the lattice spacing increase, which proves the compressive stress formation in the surface layer of as-peened material. Increment of the diffraction peaks width is known to indicate both the diminution of the grains/crystallites size and the lattice microstrains' increase. No marked changes of phase composition in VT1-0 and LCB alloys samples after the UIP were observed by the XRD analysis. The α-phase/β-phase fraction ratio was changed only slightly in the VT6 alloy. On the contrary, the strain-induced martensitic phase (the volume fraction up to 23%) is revealed in the UIP-processed samples of AISI 321 stainless steel.

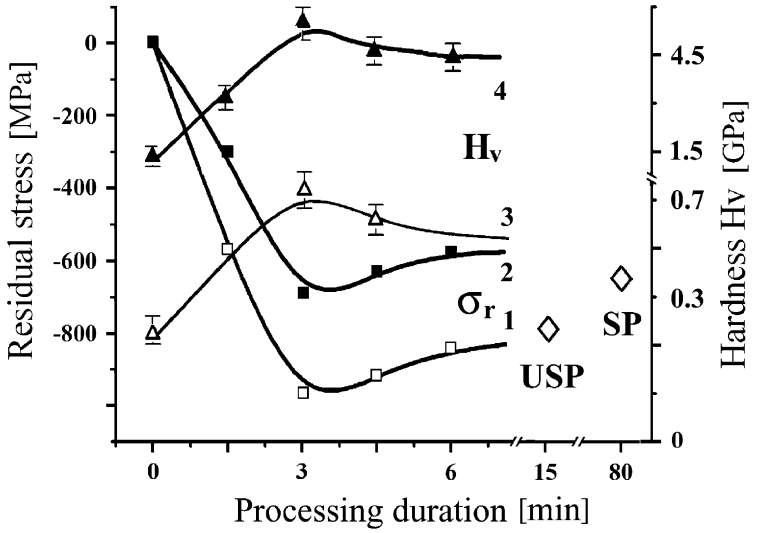

Fig. 2. Residual stresses (curves 1—□, 2—■) and Vickers' microhardness (curves 3—△, 4—▲) vs. the UIP processing duration for AISI 321 stainless steel (2—■, 4—▲) and α-titanium (VT1-0 alloy) (1—□, 3—△). Open rhombs (◇) indicate residual stress magnitudes for stainless steel processed by ultrasonic shot peening (Ref. [4]) and conventional shot peening (Ref. [34]).

Dependences of residual stresses on the processing duration estimated by the XRD analysis are shown in Fig. 2. Curves 1 and 2 indicate evolution of residual stresses in the top surface layer of the AISI 321 stainless steel samples and the VT1-0 alloy samples, respectively. The maximum magnitude is achieved after processing for 180 s in both materials, and then it slightly decreases supposedly because the deformation proceeds into deeper layers. It leads to redistribution of residual stresses through deeper layers and, in turn, to reduction of the compressive stresses' magnitude in the top surface layer. Formation of residual compressive stresses within a thin surface layer is known to be one of the most effective methods for improvement of the fatigue performance [28]. It is due to the fact that surface tensile stresses of external origin are partially nullified and reduced in magnitude by residual compressive stresses. Note, that namely the presence of processing-induced surface compressive stresses (i.e. induced by heat treatment or shot-peening procedures) is the most traditional explanation of the subsurface crack initiation (but not at the top surface) during cycling loading [1,2,28,29]. Besides, improved fatigue limit can be attributable to the ultra-fine grain structure in the top surface layer [18,30,31].

An increased Vickers micro-hardness H_v after processing revealed for studied materials (Fig. 2, curves 3,4) seems to be a result of compressive residual stresses and expected fine grain structure. Both materials demonstrate maximum values (691 MPa for α-Ti and 4.4 GPa for AISI 321 steel) after similar processing durations (about 180 s) that correlate well with minimum magnitudes of residual stresses calculated using the XRD data. Thus, it is observed that H_v of VT1-0 alloy increases twice, while much durable Ti alloys demonstrate lower hardness increase (LCB—about 40% and VT6—about 25%). Some softening of samples occurred at higher extent of plastic strain could be explained either by possible slight heating of sample during processing or by so called grain sliding effect. The latter becomes pronounced when the grain size diminishes down to magnitude of about 10 nm [32], but hardening due to the dislocation mobility is known to reduce in this case.

TEM has shown the significant grains' refinement in the top surface layers (thickness is about 10–15 μm) of as-peened samples (Fig. 3). Mainly nano-scale randomly oriented grains in the surface layer structure and indicative rings on the diffraction patterns are visible. Structure of stainless steel is characterized by average grains/crystallites size of 10–100 nm (Fig. 3a) and consists of austenitic grains and grains of the strain-induced martensite [19]. The finest grain structure is observed after the UIP in α-titanium alloy (VT1-0), and grains/crystallites size is lesser than about 10 nm (Fig. 3b). The UIP processing of $\alpha+\beta$ Titanium alloy (VT6) also leads to formation of nano scale grains/crystallite structure in the top surface layer (grain size ranges within

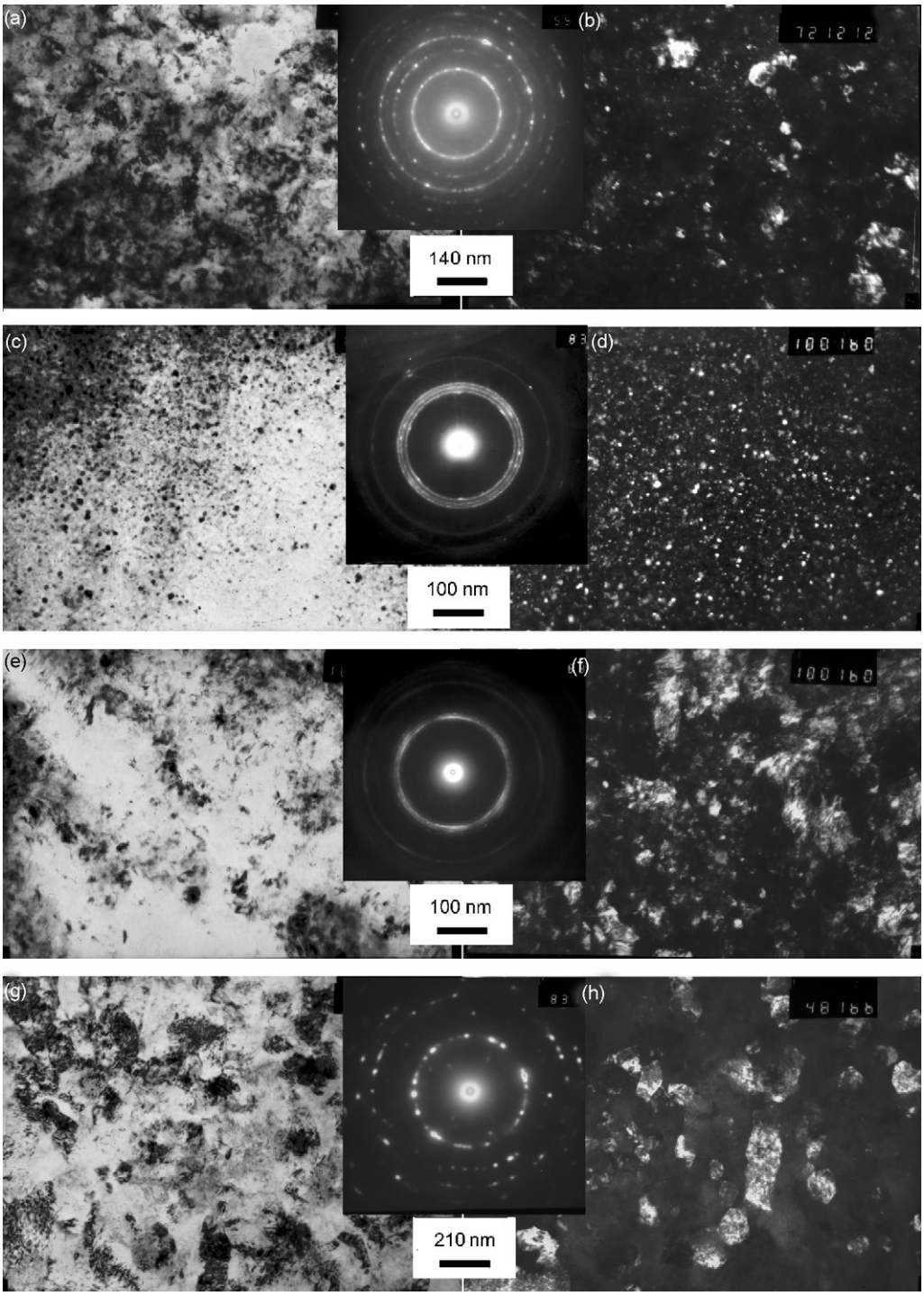

Fig. 3. TEM observations of the grain structure in the top surface layer (on the depth of about 10 μm) of metallic materials after the UIP with simultaneous shifting of sample for 4 min: (a, b) AISI 321 stainless steel, (c, d) VT1-0 titanium alloy, (e, f) VT6 titanium alloy and (g, h) LCB titanium alloy; (a, c, e, g) bright field images and (b, d, f, h) dark field images.

interval 20–100 nm). Phase composition determined by the XRD analysis remains practically unchanged. Refinement of the grain structure occurs also in β-titanium alloy (LCB), but to a lesser extent. Average grains/crystallites size of 200 nm was revealed. Such peculiarities are compatible with the data reported in Ref. [31],

which showed that fatigue response of metastable titanium alloys (such as LCB) to shot peening is significantly less beneficial than that for $\alpha+\beta$ titanium alloys (for instance Ti–6Al–4V).

Obtained results indicate that the UIP can be considered as another powerful method for management of surface properties. Beneficial characteristics of surface layers promoting the enhanced fatigue behavior can be achieved by the UIP for relatively short periods of time in comparison with traditional surface treatment techniques. The results of fatigue tests for samples processed both by the UIP and by other surface treatments are listed in Table 2.

The most indicative results are obtained in this study for welded samples of low carbon steel (Fig. 4). The TEM observations of structure in the top surface layer of the processed welded joint reveal the nano-scale grain structure, and diffraction pattern is indicative in this sense (Fig. 4b). The fatigue behavior of as-welded sample was examined first (Fig. 4a, curve 1), and the fatigue limit was determined. Then, the welded joint area was processed by the UIP using scheme A (Fig. 1a, Table 1). Then, high cycle fatigue tests of processed sample were carried out. Moreover, one series of fatigue samples was UIP-processed directly after welding (Fig. 4, curve 2), but other series was UIP-processed after prior cycling up to 50% of as-welded sample fatigue life (Fig. 4, curve 3). The latter samples demonstrate even more improved fatigue behavior than that processed directly after welding. This feature can be explained by partial relaxation of tensile residual stresses in the welded joint during preliminary cycling. The effect of the UIP becomes more pronounced after this prior relaxation.

Evidently, the surface roughness should be considered as another important factor affecting to the fatigue durability. Indeed, rough surface created by the SPD processing may induce stress concentration at specific points, thereby facilitating the fatigue crack initiation. Indicative data are listed in Table 2, which describe the

Table 2
Fatigue performance of metallic materials after the surface treatment by different peening techniques

Material	Peening method, processing duration (min)	Grain structure in surface layer D_{av} (nm)	Surface roughness, R_a (μm)	Fatigue performance in as-processed condition, σ_a, MPa and N, cycles	Reliability increment vs. pristine $\Delta\sigma_a$ (MPa)	Refs.
316L stainless steel	USP/SMAT[a], 30–60	20	—	380 MPa at 2×10^6 cycles	80 MPa (21%)	[30]
316L stainless steel	UIP[b], 4	20–30	2–3	—	—	Present work, [19]
Low carbon steel	USP/HESP, 30–180	23–33	—	—	—	[5]
Low carbon steel (weld)	UIP, 5	30–50	~10	185 MPa at 2×10^6 cycles	60 MPa (50%)	Present work
4340 Steel	SP[c], 90	—	—	460 MPa at 4×10^6 cycles	57 MPa (14%)	[12]
VT1-0 (α-titanium)	UIP, 4	<10	~2	307 MPa at 1.5×10^7 cycles	95 MPa (39%)	Present work, [18]
VT1-0 (α-titanium)	—	—	Electro-polished	250 MPa at 1×10^6 cycles	−80 MPa (−30%)	[22]
			Micro-pitted (hole 0.25 mm)	170 MPa at 1×10^6 cycles		
Ti6Al4V $\alpha+\beta$-Ti alloy	—	~10000	Smooth	520 MPa at 1×10^6 cycles	−170 MPa (−50%)	[20,21]
			Pitted by 3 mm shot	350 MPa at 1×10^6 cycles		

[a]USP/SMAT/HESP—ultrasonic shot peening/surface mechanical attrition treatment/high energy shot peening.
[b]UIP—ultrasonic impact peening.
[c]SP—shot peening.

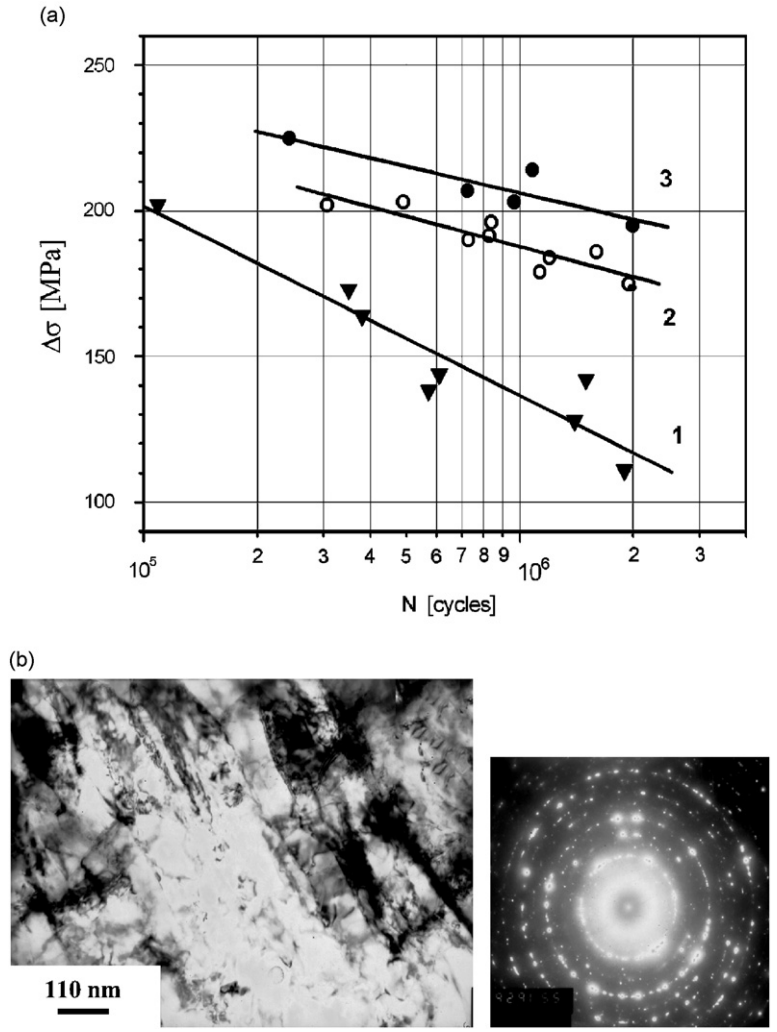

Fig. 4. Fatigue behavior of low carbon steel welds (a) and TEM bright field image of structure with diffraction pattern in top surface layer of weld after the UIP (b): (1—▼) in as-welded conditions, (2—○) after UIP processing directly after welding, (3—●) after the UIP processing after prior cycling up to 50% of the fatigue life of as-welded sample.

fatigue performance of smooth and notched or micro-pitted samples of CP-titanium (VT1-0 alloy) [22] and even more durable $\alpha+\beta$-titanium alloy (Ti6Al4V) [20,21].

Apparently, one should try to choose the processing regime providing the resulting surface roughness magnitude to be as lower as possible. In this connection, we will demonstrate further that the UIP processing proposed here allows obtaining the smoother surface relief in comparison with that after random repeated impacts in almost vertical directions occurred at other peening methods.

Experimentally, the surface roughness of stainless steel samples was measured by profilometry after the UIP processing (scheme A) during 60, 120 and 240 s. The resulting surface profiles are shown in Fig. 5(b–d) in comparison with the initial state (Fig. 5a). An evolution of the measured arithmetic mean value R_a characterizing surface roughness is shown in Fig. 5e, which indicates some qualitative similarity with such dependence for the case of shot peening reported in Ref. [7]. The R_a magnitudes obtained in Ref. [7] are slightly higher because the Al alloy was studied there. However, the dependence remains qualitatively the same, namely the surface roughness increases sharply at the beginning stage of treatment, further it achieves maximum value, and then it decreases and achieves some saturation magnitude. It should be noticed that the time, which is necessary to saturation, is much lower for the UIP than that for the shot peening. This feature

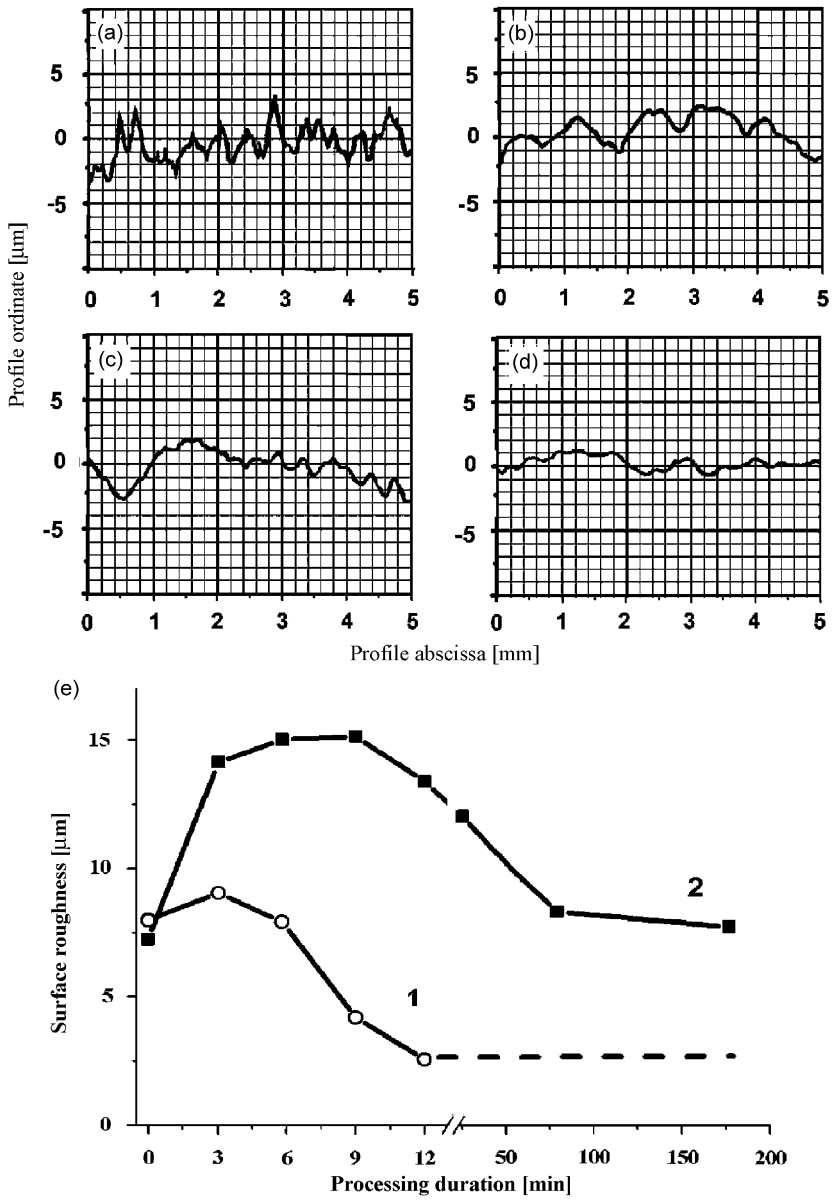

Fig. 5. Evolution of the surface roughness obtained by profilometry under the UIP processing: (a) surface profile of initial sample, (b, c, d) surface profiles after the UIP with simultaneous shifting of the impact head for 60 s (b), 120 s (c) and 240 s (d), (e) dependence of the surface roughness (the arithmetic-mean R_a value) on the processing duration measured experimentally from the stainless steel plate processed by the UIP (curve 1 (○)) and the Al alloy plate impacted with 7.9 mm WC/Co balls (curve 2 (■) is taken from Ref. [7]).

becomes explainable if one consider the random character of impactions at shot peening, thus much time is necessary to obtain the 100% coverage of the treated surface [7,25,33]. On the other hand, the UIP permits producing more controllable processing regime [18], consisting in controllable magnitude of the lateral load component during single impaction. The fact that lateral load component should lead to smoother surface seems sufficiently evident. However, for accurate determination of optimum processing regime one should use more accurate calculations, for example FEM analysis [7,25,33].

For this purpose a FE model is used in order to evaluate the indent contours formed on the AL alloy sample surface after impaction by a rigid ball. Currently, FE model described in Section 2.3 is incapable to predict the surface roughness evolution during the UIP processing. However, it evidently shows the distinct influence of

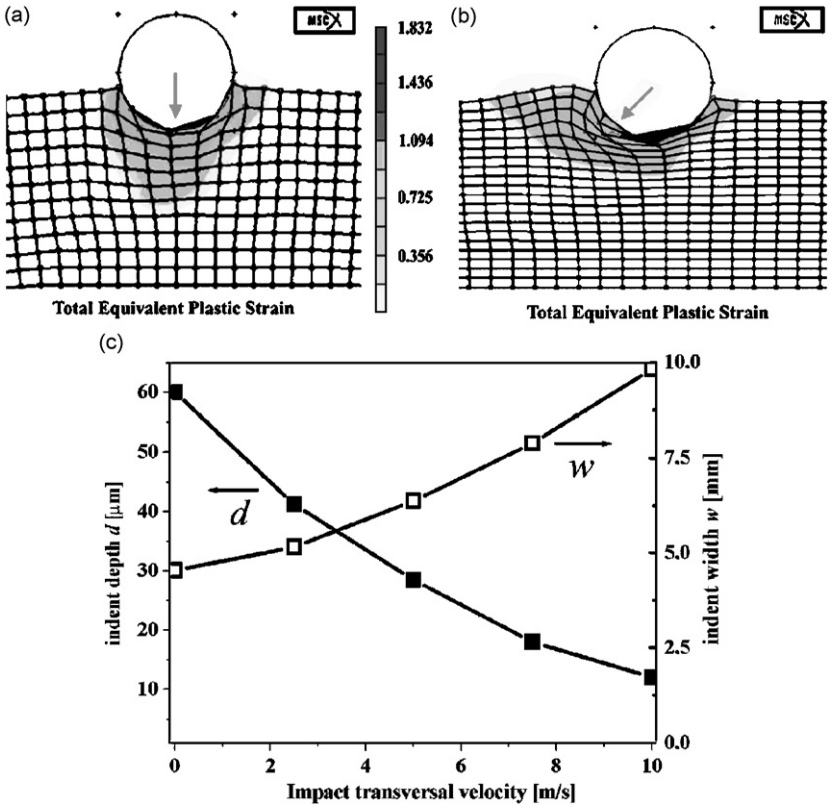

Fig. 6. Equivalent plastic strain meshes for single indents modeled using FE code MSC Marc 2005: (a) impaction at vertical (90°) direction, (b) impaction at inclined (45°) direction, (c) dependencies of the indent depth (■) and the indent width (□) on the lateral velocity magnitude.

the magnitude of the lateral load component operated during single impaction on the crater depth and width. It is seen in Fig. 6, which shows the total equivalent plastic strain meshes for two cases. The first one (Fig. 6a) is obtained for impaction in vertical (90°) direction to the impacted surface, while the other one (Fig. 6b) is obtained for impaction with simultaneous vertical and lateral load components. The mesh shown in Fig. 6b is calculated at the load components ratio 50:50. The crater contours simulated for single impact indicate that the shot with lateral load component (''sliding'' impaction) promotes a significantly larger plastic pile-up at the exit side of the crater, whereas the vertical (90°) shot results in the symmetric crater (and symmetric pile-ups). Moreover, the depth of the crater formed at ''sliding'' impaction becomes smaller and its width increases, when the magnitude of the lateral load component increases (Fig. 6c). Thus, in present simulation we have observed features resembling to those obtained for the case of inclined shots reported in Refs. [20,21].

4. Summarizing remarks

This study shows that the UIP technique, which provides severe plastic deformation via repetitive ''sliding'' impacts, may produce a number of beneficial properties of surface layers in different metallic materials. They are the following: (i) nanocrystalline structure (in a layer at least of about 10 μm thick); (ii) surface compressive residual stresses (down to −700 and −1000 MPa for AISI 321 stainless steel and α-titanium, respectively); (iii) work hardening of the surface layer (H_v up to 4.4 GPa and 691 MPa for AISI 321 stainless steel and α-titanium, respectively). These enhanced properties of the surface layer are shown to be attribute to the obtained superior fatigue behavior of processed materials (including welded joints) during high-circle fatigue tests.

Besides, both profilometry and 2D FE simulations show that the UIP technique proposed may results in the reduced surface roughness due to "sliding" impacts caused either by the purposeful impact head rotation or by low-frequency vibrations of sample itself. The FE modeling based on the indentation of a rigid high-velocity pin impacting an elasto-plastic surface also shows that the thickness of the deformed layer depends on the pin lateral velocity.

Thus, the FE modeling in the conjunction with the microstructural analysis results shows that the optimal pin lateral velocity can be chosen considering two competitive factors, namely the decreasing of the surface roughness and diminution of thickness of the nanocrystalline surface layer. At the same time, the higher the "sliding" velocity of pin the lower the indent depth and the thinner the hardened nanocrystalline surface layer. Moreover, the refinement of the surface structure down to nano-scale range may not be induced at all if the impacted energy of pins is not large enough due to excessively high lateral velocity.

However, the FE model requires further debugging for 3D case in order to determine the surface roughness evolution with the treatment time and to obtain more reliable predictions.

Acknowledgements

This study was partially supported by National Academy of Sciences of Ukraine and the Fundamental Research Program "Nanosystems, Nanomaterials and Nanotechnologies". Authors would like to thank Dr. V.V. Knysh from Paton Welding Institute for his help in fatigue testing of welded samples. BNM acknowledges the support of the Science and Technology Center in Ukraine (Project # 3520).

References

[1] A.M. Sulima, M.I. Yevstigneev, *Quality of Surface Layer and Fatigue Durability of Details Made from Heatproof and Titanium Alloys*, Machine building, Moscow, 1974 (in Russian).
[2] L Wagner, Mechanical surface treatments on titanium, aluminum and magnesium alloys, *Materials Science and Engineering A* 263 (1999) 210–216.
[3] K. Lu, J. Lu, Surface nanocrystallization of metallic materials—presentation of the concept behind a new approach, *Journal of Materials Science and Technology* 15 (3) (1999) 193–197.
[4] G. Liu, J. Lu, K. Lu, Surface nanocrystallization of 316L stainless steel induced by ultrasonic shot peening, *Materials Science and Engineering A* 286 (2000) 91–95.
[5] G. Liu, S.C. Wang, X.F. Lou, K. Lu, J. Lu, Low carbon steel with nanostructured surface layer induced by high-energy shot peening, *Scripta Materialia* 44 (2001) 1791–1795.
[6] K.Y. Zhu, A. Vessel, F. Brisset, K. Lu, J. Lu, Nanostructure formation mechanism of α-titanium using SMAT, *Acta Materialia* 52 (2004) 4101–4110.
[7] K. Dai, J. Villegas, Z. Stone, L. Shaw, Finite element modeling of the surface roughness of 5052 Al alloy subjected to a surface severe plastic deformation process, *Acta Materialia* 52 (2004) 5771–5782.
[8] L. Wagner (Ed.), *Proceedings of ICSP-8 on Shot Peening*, Wiley-VCH, Weinheim, 2003.
[9] H. Lee, S. Mall, S. Sathish, Investigation into effects of re-shot-peening on fretting fatigue behavior of Ti–6Al–4V, *Materials Science and Engineering A* 390 (2005) 227–232.
[10] G.I. Prokopenko, A.V. Kozlov, J.I. Kleiman, P.P. Micheev, V.V. Knysh, Yu.F. Kudryavtsev, Device for ultrasonic peening of metals, US Patent no. 6,467,321, 2002.
[11] L.V. Lobanov, P.P. Mikheev, G.I. Prokopenko, V.V. Knysh, Yu.F. Kudryavtsev, Ja.I. Kleiman, B.N. Mordyuk, Method for processing welded metal work joints by high-frequency hammering, US Patent Application #Al 20040244882, December 9, 2004.
[12] P.E. Haagensen, Fatigue of high strength steels, *Proceedings of Second International Symposium on High Strength Steel*, Verdal, Norway, 2002.
[13] N.A. Krylov, A.M. Polischuk, The use of ultrasonic equipment for metal structure stabilization, *Basic Physics of Industrial Ultrasonic Applications, Part 1* (1970) 70 (in Russian).
[14] C.-C. Feng, K. Graff, Impact of spherical tool against a sonic transmission line, *Journal of Acoustic Society of America* 52 (1) (1972) 254–262.
[15] V.A. Kotko, G.I. Prokopenko, S.A. Firstov, Structure changes in Mo hardened using ultrasound, *Soviet Physics Metallurgy Materials* 37 (2) (1974) 444–445 (in Russian).
[16] E.Sh. Statnikov, E.M. Shevtsov, V.F. Kulikov, Ultrasonic impact tool for strengthening welds and reducing residual stresses, Scientific Transactions, *Metallurgiya*, No. 92, Moscow, 1977, p. 107 (in Russian).
[17] G.I. Prokopenko, M.O. Vasylyev, B.N. Mordyuk, G.I. Kuzmich, O.F. Lugovskoy, V.I. Chorniy, Ultrasonic device for hardening and nanostructurization of the metallic surfaces, Ukrainian Patent no. 9175, 2005 (in Ukrainian).

[18] B.N. Mordyuk, G.I. Prokopenko, Fatigue life improvement of α-titanium by novel ultrasonically assisted technique, *Materials Science and Engineering A* 437 (2006) 396–405.
[19] B.N. Mordyuk, G.I. Prokopenko, M.O. Vasylyev, M.O. Iefimov, Effect of structure evolution induced by ultrasonic peening on corrosion behavior of AISI-321 stainless steel, *Materials Science and Engineering A* 458 (2007) 253–261.
[20] J.O. Peters, B.L. Boyce, X. Chen, J.M. McNaney, J.W. Hutchinson, R.O. Ritchie, On the application of the Kitagawa–Takahashi diagram to foreign-object damage and high-cycle fatigue, *Engineering Fracture Mechanics* 69 (2002) 1425–1446.
[21] J.O. Peters, R.O. Ritchie, Foreign-object damage and high-cycle fatigue of Ti–6Al–4V, *Materials Science and Engineering A* 319–321 (2001) 597–601.
[22] J.-H. Kim, M.-G. Kim, Considerations in non-propagating crack of pure titanium, *Materials Science and Engineering A* 346 (2003) 216–222.
[23] A.C. Sekkal, C. Langlade, A.B. Vannes, Tribologically transformed structure of titanium alloy (TiAl6V4) in surface fatigue induced by repeated impacts, *Materials Science and Engineering A* 393 (2005) 140–146.
[24] G.I. Prokopenko, T. Lyatun, Investigation of regimes of ultrasonic surface hardening, *Soviet Physics and Chemistry of Treatment of Materials* (1974) 91–95 (in Russian).
[25] M. Frija, T. Hassine, R. Fathallah, C. Bouraoui, A. Dogui, Finite element modelling of shot peening process: prediction of the compressive residual stresses, the plastic deformations and the surface integrity, *Materials Science and Engineering A* 426 (2006) 173–180.
[26] MSC. Software GmbH, MSC. Marc/Introductory Course, 2003.
[27] C.Y. Ho, (Ed.), J.M. (Tim) Holt (Technical Ed.), Structural Alloys Handbook, CINDAS/Purdue University, West Lafayette, IN, 1996.
[28] A. Sollich, H. Wohlfahrt, Optimization of the fatigue strength of heat treated steels as a consequence of an optimum state of the surface and of subsurface layers after shot peening, *Proceedings of the Sixth International Conference on Shot Peening*, San Francisco, USA, 1996, pp. 251–262.
[29] M. Ya, Y. Xing, F. Dai, K. Lu, J. Lu, Study of residual stress in surface nanostructured AISI 316L stainless steel using two mechanical methods, *Surface and Coating Technology* 168 (2003) 148–155.
[30] T. Roland, D. Retraint, K. Lu, J. Lu, Fatigue life improvement through surface nanostructuring of stainless steel by means of surface mechanical attrition treatment, *Scripta Materialia* 54 (2006) 1949–1954.
[31] L.Wagner, M. Kocan, T. Ludian, Fatigue response of the various titanium alloy classes to shot peening, Metal Finishing News, No. 5, 2004, 〈http://www.mfn.li/article/?id=229〉.
[32] J. Schiøtz, T. Vegge, F.D. Di Tolla, K.W. Jacobsen, Atomic-scale simulations of the mechanical deformation of nanocrystalline metals, *Physical Review B* 60 (1999) 11971–11983.
[33] A. Levers, A. Prior, Finite element analysis of shot peening, *Journal of Material Processing Technology* 80–81 (1998) 304–308.
[34] H. Guechichi, L. Castex, Fatigue limits prediction of surface treated materials, *Journal of Material Processing Technology* 172 (2006) 381–387.